RSC Advances

PAPER

View Article Online
View Journal | View Issue



Cite this: *RSC Adv.*, 2014, **4**, 40606

# Theoretical and experimental studies of the corrosion inhibition effect of nitrotetrazolium blue chloride on copper in 0.1 M $H_2SO_4$

Anmin Liu,[a] Xuefeng Ren,[a] Jie Zhang,[a] Chong Wang,[a] Peixia Yang,[a] Jinqiu Zhang,[a] Maozhong An,*[a] Drew Higgins,[b] Qing Li[b] and Gang Wu*[bc]

Received 3rd June 2014
Accepted 26th August 2014

DOI: 10.1039/c4ra05274a

www.rsc.org/advances

The inhibition effect of nitrotetrazolium blue chloride (NTBC) on copper corrosion in 0.1 M $H_2SO_4$ solution was investigated by quantum chemical calculations, molecular dynamic (MD) simulations, electrochemical measurements, and scanning electron microscopy (SEM) surface morphological examination. X-ray photoelectron spectroscopy (XPS) measurements were also employed to study the adsorbed layer of NTBC on the copper surface. Adsorption behaviors of NTBC on copper surfaces were studied by MD simulations. The inhibition effect of NTBC was further confirmed by the results of electrochemical measurements and surface morphological examination. The NTBC increased the total resistance of the copper corrosion process according to the results of EIS due to formation of an absorption layer on the copper surface. Potentiodynamic polarization curves indicated that the corrosion rate decreased prominently with the addition of NTBC into $H_2SO_4$ solution, as the increasing concentration of NTBC caused a decreasing current density ($i_{corr}$). The optimal concentration of NTBC as an inhibitor for the corrosion of copper in 0.1 M $H_2SO_4$ solutions was determined to be 500 ppm according to electrochemical and morphological studies. Quantum chemical calculations were employed to study the electronic properties of NTBC to ascertain the correlation between the inhibitive effect and the molecular structure. Both the experimental and theoretical results are in good agreement with each other in this regard and confirm that NTBC is an effective inhibitor. The quantum chemical calculations and MD simulations provided strong evidence that the superior inhibition effect of NTBC is due to its ability to adsorb strongly at copper surfaces.

## 1. Introduction

Copper is a widely used metal in interconnects of advanced microelectronic devices or heating and cooling systems due to its excellent electrical and thermal conductivity, along with good mechanical workability.[1–3] Unfortunately, copper corrosion is a process that causes many detrimental issues throughout a wide array of industrial applications. The uses of corrosion inhibitors that aim to minimize corrosion or prevent it from occurring, is one of the most practical methods for protecting metals against degradation by oxidation, especially in acidic media.[4–6] Many efficient inhibitors containing O, N, or S atoms and heterocyclic structures can significantly reduce the occurrence of corrosion with the addition of only very small amounts.[4,6–9]

To date, the inhibition mechanism of organic corrosion inhibitors has not been clearly elucidated yet. However, it is generally accepted that, in most cases, the inhibition of corrosion is achieved through the interaction of inhibitor molecules with the metal surfaces (*i.e.* copper).[10–14] This results in a formation of an inhibitive surface film, creating coordinate bonds between copper ions with vacant "d" orbitals and atoms with the ability to donate electrons.[3,7] Traditionally, experimental methods such as polarization curves, electrochemical impedance spectroscopy, morphology measurements, and weight loss assessment were sophisticatedly employed to screen various inhibitors and study their inhibiting performance.[15–17] However, these experimental methods have inherent limitations including blindness, workload, as well as time and resource waste. In the last decades, quantum chemistry,[18–21] computational chemistry[22–24] and molecular dynamic simulation[25–27] have rapidly emerged for the calculation,[28] modeling[29] and simulation[30] of small chemical[31] and biological[32] systems as a technique to understand and predict behaviors at the molecular level. Therefore, combining computational chemistry

[a]*State Key Laboratory of Urban Water Resource and Environment, School of Chemical Engineering and Technology, Harbin Institute of Technology, Harbin, 150001, China. E-mail: mzan@hit.edu.cn; Tel: +86-451-86418616*

[b]*Materials Physics and Applications Division, Los Alamos National Laboratory, Los Alamos, New Mexico 87545, USA*

[c]*Department of Chemical and Biological Engineering, University at Buffalo, The State University of New York, Buffalo, New York 14260, USA. E-mail: gangwu@buffalo.edu*

predictions with experimental investigation and validation has emerged as a highly efficient methodology for accelerating the development of novel inhibitor species.[33–36]

Among all the computational chemistry methods, quantum chemical calculations[35,37–40] and molecular dynamic simulations[41–43] have been widely used to investigate the molecular configuration, electronic structures, reactivity of the corrosion inhibitors and the interactions between the inhibitor molecules and the metal surfaces.[12,13,28,38,44,45] The highest occupied molecular orbital (HOMO) and lowest unoccupied molecular orbitals (LUMO) eigenvalues, the HOMO–LUMO gap, and the Fukui functions[46–48] are the most commonly used parameters to interpret the interaction mechanisms occurring between organic inhibitors and metal surfaces at the atomic level. Molecular dynamic simulations are also commonly employed to study the adsorption interactions between organic inhibitor molecules and metal surfaces, and can provide insight into the design of inhibitor systems with superior properties and interaction energies, which can be interpreted to explain the difference of inhibition efficiency between organic inhibitors.[49–51] Particularly, high binding energy values mean that organic inhibitor molecules will give high inhibition efficiency.[12,52–54]

In the present work, molecular dynamic simulations were employed to study the adsorption behavior of NTBC on the copper surface. The inhibition effect of nitrotetrazolium blue chloride (NTBC) for copper corrosion in 0.1 M $H_2SO_4$ has been studied with potentiodynamic polarization and electrochemical impedance spectroscopy (EIS) techniques. Results of EIS revealed that the NTBC increased the whole resistance of copper corrosion process by forming an absorption layer on copper surface. Potentiodynamic polarization curves confirmed that the corrosion rate decreased prominently with the addition of NTBC in $H_2SO_4$ solution, as the increasing concentration of NTBC caused a decreasing current density ($i_{corr}$). SEM images support that the NTBC inhibited the corrosion of copper surface. The saturated concentration of NTBC as an inhibitor for the corrosion of copper in 0.1 M $H_2SO_4$ solutions was 500 ppm.

In the meantime, the relationship between the molecular structures and corrosion inhibition effect of NTBC was established by quantum chemical calculations. According to the quantum chemical calculations, the N atoms in the imidazole ring were the most active adsorption sites and NTBC most likely acts as an effective inhibitor by binding to the copper surface.

## 2. Experimental

### 2.1. Quantum chemical calculations and MD simulations

MD simulations were carried out in a simulation box with periodic boundary conditions using Materials Studio 6.0 (from Accelrys Inc.). The box consisted of a copper surface (with 6 layers of copper atoms cleaved along the (111) plane, as the cut off radius of MD simulations is 0.95 nm), with a size of 3.067 nm × 3.067 nm × 1.043 nm, angles of 90° × 90° × 120° of Cu, and a liquid phase and vacuum layer of 1 nm height. During the simulation, all 6 layers of copper atoms were fixed. The liquid phase was composed of water molecules with a density of 1 g $cm^{-3}$ and one organic inhibitor molecule. The simulation was carried out using discover module with a time step of 1 fs and simulation time of 500 ps performed at 298 K, NVT ensemble, and an *ab initio* polymer consistent force field (PCFF).[55–58]

The interaction energy was calculated using eqn (1).

$$E_{interaction} = E_{total} - E_{copper} - E_{inhibitor} \quad (1)$$

where $E_{total}$ was the total energy of the copper crystal together with the adsorbed organic inhibitor. $E_{copper}$ and $E_{inhibitor}$ were the total energy of the copper crystal and free inhibitor, respectively. The binding energy was the negative value of the interaction energy.

Quantum chemical calculations were performed by the DFTB+ (based on the Density Functional Tight Binding (DFTB)) and DMol$^3$ module in Materials Studio 6.0 (from Accelrys Inc.).[59–63] Electronic properties and orbital information of NTBC were calculated by using the Becke, Lee, Yang and Parr (BLYP)[64–66] model and DFTB+ method, respectively. In the DFTB+ method, self-consistent charges and 1E-008 SCC Tolerance were used for the quantum chemical calculations.

### 2.2. Measurements and apparatus

X-ray photoelectron spectra (XPS) measurements were employed to study the adsorbed layer of NTBC on the copper surface. The XPS spectra were taken using PHI 5700 ESCA System (Perkin-Elmer, USA) at room temperature. The excitation source was Al Kα radiation (photoelectron energy, 1486.6 eV). The photoelectrons were detected with a hemispherical analyzer. The inhibiting inhibition effect of NTBC on copper surfaces was evaluated by potentiodynamic polarization (Tafel curves), EIS techniques, and Scanning Electron Microscope (SEM) images. All electrochemical measurements were carried out in a conventional three electrode system, using a copper foil as the working electrode, a Pt plate as the auxillary electrode and a saturated mercurous sulfate electrode (SSE) as the reference electrode.

Potentiodynamic polarization curves were obtained by changing the electrode potential automatically from ±250 mV *via* OCP *vs.* SSE with a scan rate 1.0 mV $s^{-1}$ at 298 K.

Inhibition efficiency ($\eta_p$) was calculated by eqn (2):

$$\eta_p = \frac{i_{corr(0)} - i_{corr(i)}}{i_{corr(0)}} \times 100\% \quad (2)$$

where $i_{corr(0)}$ and $i_{corr(i)}$ were uninhibited and inhibited corrosion current densities, respectively.

EIS measurements were carried out at open-circuit potential with potential amplitude of 5 mV, at room temperature (298 K). The inhibition efficiency ($\eta_I$) was calculated by charge transfer resistance, as displayed in eqn (3):

$$\eta_I = \frac{R_{ct(i)} - R_{ct(0)}}{R_{ct(i)}} \times 100\% \quad (3)$$

where $R_{ct(0)}$ and $R_{ct(i)}$ are the charge transfer resistance values without and with inhibitors, respectively.

Field emission scanning electron microscopy was used to reveal the surface morphological changes of copper surface after corrosion experiment. Copper foils were immersed in 0.1 M $H_2SO_4$ solution in the presence and absence of inhibitors for 24 hours at 298 K. Then, these foils were cleaned with distilled water, dried by cold air, and further studied using SEM.

# 3. Results and discussion

## 3.1. Molecular dynamic simulation

MD simulation was performed to study the adsorption behavior of NTBC on Cu (111) surfaces with results displayed in Fig. 1. Fig. 1(a) shows the initial configuration of the MD simulation box, with the NTBC placed near the copper surface. The equilibrium configuration of the MD simulation box after simulating for 500 ps is illustrated in Fig. 1(b). The

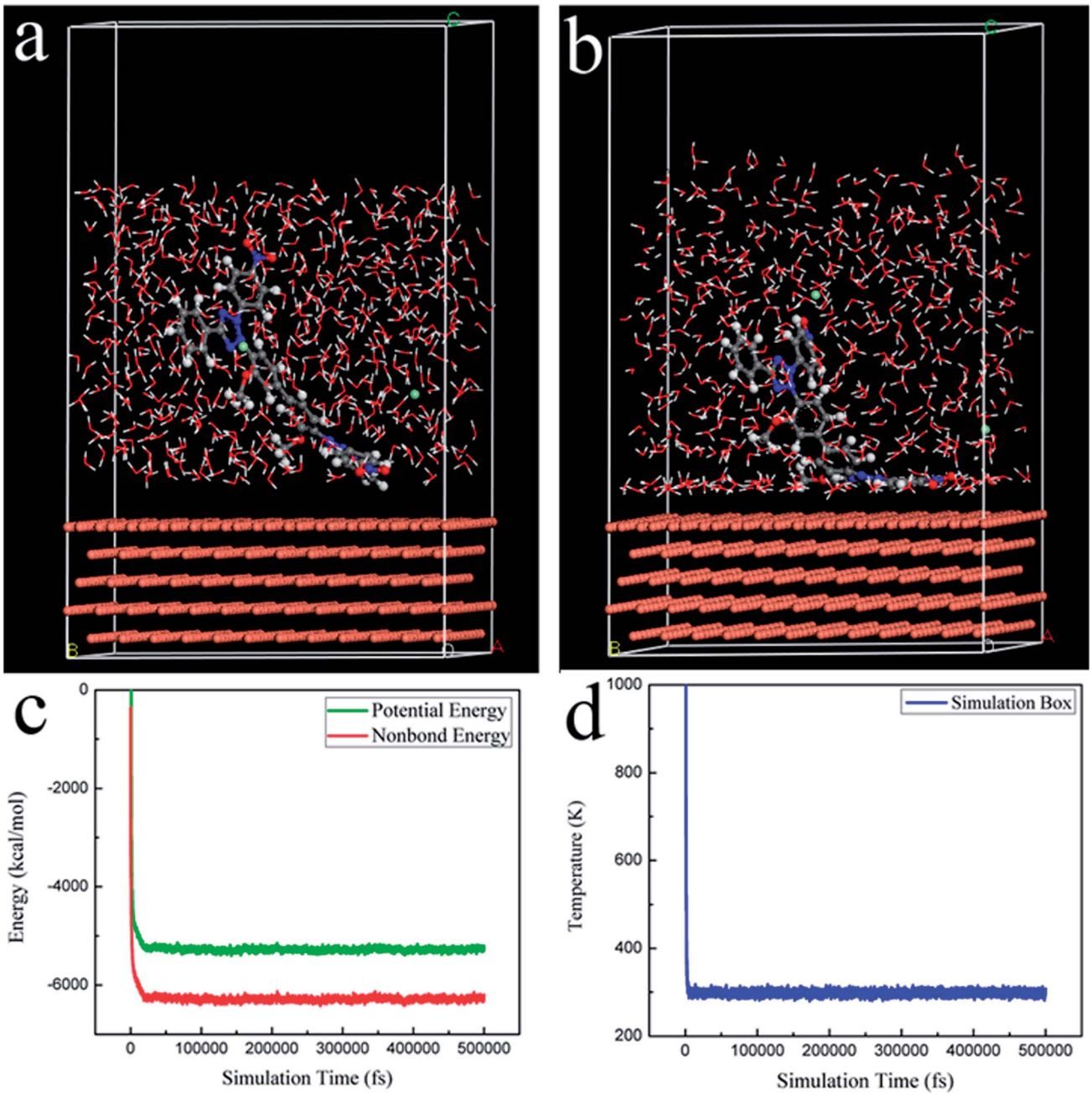


Fig. 1 (a) Initial configuration of the MD simulation box (NTBC was visualized by balls and sticks, and water molecule by lines). (b) Final equilibrium configuration of the MD simulation box (adsorption behavior of NTBC on the Cu surface). (c) Energy fluctuation curves of the MD simulation. (d) Temperature fluctuation curve of the MD simulation.

 

energy and temperature fluctuation curves in Fig. 1(c) and (d) of the MD simulation indicated that the simulation system was already at equilibrium when the calculations stopped. The $E_{binding}$ value calculated from Fig. 1(b) was 404.790 kJ mol$^{-1}$, indicating an effective adsorption of NTBC on the copper surface and a correspondingly adsorbed layer of NTBC on the copper surface. The binding energy of NTBC on the copper surface is very high, suggesting that there is more than one bond to the copper surface per NTBC molecule.[67] The prediction was confirmed by following XPS measurement and quantum chemical calculations. Electrochemical measurements and copper corrosion experiments were also carried out to confirm this prediction.

### 3.2. Adsorption of NTBC on the copper surface

The prepared copper sample with a cleaned surface was immersed in the 1000 ppm NTBC aqueous solution for 24 hours. The immersed sample used for XPS measurement was rinsed with deionized water and then dried with a gentle flow of air. The XPS survey scan was taken over a wide binding energy region from 1.200–1350.000 eV that indicated the presence of carbon, nitrogen, oxygen, chlorine, and copper species. The binding energy of the C1s peak at 284.6 eV was used as an internal standard.

Fig. 2(a) displayed the general spectra of the original copper surface immersed in the 1000 ppm NTBC aqueous solution for 24 hours and the surface after 10.0 nm etching during the XPS analysis. The detailed XPS peak of N1s from the original immersed copper surface was shown in Fig. 2(b). High resolution Cu2p peaks of the immersed copper surface and a 10.0 nm depth of the copper surface were shown in Fig. 2(c). Meanwhile, Fig. 2(d) showed the detailed N1s peak after 10.0 nm etching of the immersed copper surface.

As displayed in Fig. 2(a) and (b), obvious signals for C, N, O, and Cl can be detected at the immersed copper surface, indicating an adsorbed layer on the copper surface. The high resolution N1s peaks indicated the presence of several chemically nonequivalent nitrogen atoms on the copper surface. Four distinct peaks were found at the binding energy of 399.4, 400.9, 403.5 and 405.6 eV. The peak at the binding energy of 405.6 eV can be attributed to the nitrogen atoms in the nitro groups of NTBC.[68,69] The peak at the binding energy of 403.5 eV can be assigned to the quaternary nitrogen atoms in NTBC.[70] The peaks at 399.4 eV and 400.9 eV can be attributed to C–N or C=N bonds, and N–N or N=N bonds in the tetrazole ring in NTBC, respectively.[71–73] Thus, the significant N1s peaks indicate the presence of NTBC on the copper surface, suggesting that NTBC can be strongly adsorbed on the copper surface when the copper is immersed in the NTBC aqueous solution. Four N1s peaks of NTBC on the copper surface revealed that more than one bond to the copper surface per NTBC molecule, confirmed the prediction of MD simulation.

Moreover, as demonstrated in Fig. 2(c) and (d), after 10.0 nm etching of the copper surface, the signal of Cu was significantly enhanced, compared with that of the original immersed copper surface. The significant XPS peak of N1s after 10.0 nm etching of the immersed copper surface revealed an effective adsorption of NTBC on the copper surface. The combination of XPS measurements and the structure with two symmetric heterocyclic groups and two quaternary ammoniums showed that NTBC can strongly adsorb on the copper surface.

### 3.3. Electrochemical impedance spectroscopy (EIS)

The inhibition effect of NTBC on copper surfaces was evaluated using electrochemical measurements. In order to study the inhibition effect of NTBC on copper in 0.1 M $H_2SO_4$ medium, EIS measurements were carried out under various concentrates of NTBC at 298 K. The Bode magnitude plots, Bode phase angle plots, and Nyquist plots are displayed in Fig. 3, 4, and 5, respectively.

The Bode magnitude plots (displayed in Fig. 3) showed that the impedance spectra obtained from the measurements as a function of concentrations of NTBC oscillate in a narrow range (from the logarithmic values of about 3.05–3.45) at the lowest frequency. These results indicate that the adsorption of NTBC on the copper surface possesses a similar inhibiting mechanism over the whole concentrations.

As displayed in Fig. 4, the Bode phase angle plots of the short-term coupons have an apparent maximum angle with a small shoulder. The maximum angles appearing in the frequency range of 1 to 100 Hz are ascribed to the formation of an adsorption of NTBC on the copper surface; the small shoulder located in the frequency range between 0.5 and 1 Hz is probably associated with the electrical double layer. The phase maxima in the Bode phase angle plots usually provide information on the relaxation time constants. Here, the Bode phase angle plots for NTBC on the copper corrosion experiments thus reveal the existence of two time constants.[74–76]

An equivalent circuit is shown in Fig. 6, considering all processes involved in the electrical response of the system.

$R_s$ is the resistance corresponding to the ohmic resistance of the system. $C_d$, is a constant phase element that is representative of the double layer capacity. $R_{ct}$ represents the resistance of charge transfer process during the corrosion of copper. The value of $R_{ct}$ corresponds to the corrosion inhibition ability of solutions with various concentrations of NTBC. $Q_A$ and $R_A$, related to the absorption behavior of NTBC on copper surface, represent the adsorption quantity and the inhibitor's resistance induced by the adsorption of NTBC on copper surface, respectively. The values of all elements obtained by fitting are listed in Table 1.

On the basis of analysis of the Nyquist plots (Fig. 5), a depressed capacitive loop rose from the time constant of the electric double layer, charge transfer resistance, and the adsorption of NTBC on copper surface. Obviously, the diameters of the capacitive loop with NTBC as inhibitor were bigger than in the absence of NTBC. Moreover, the diameters increased with the increments of the inhibitor concentration. These results indicated that the corrosion inhibition ability of

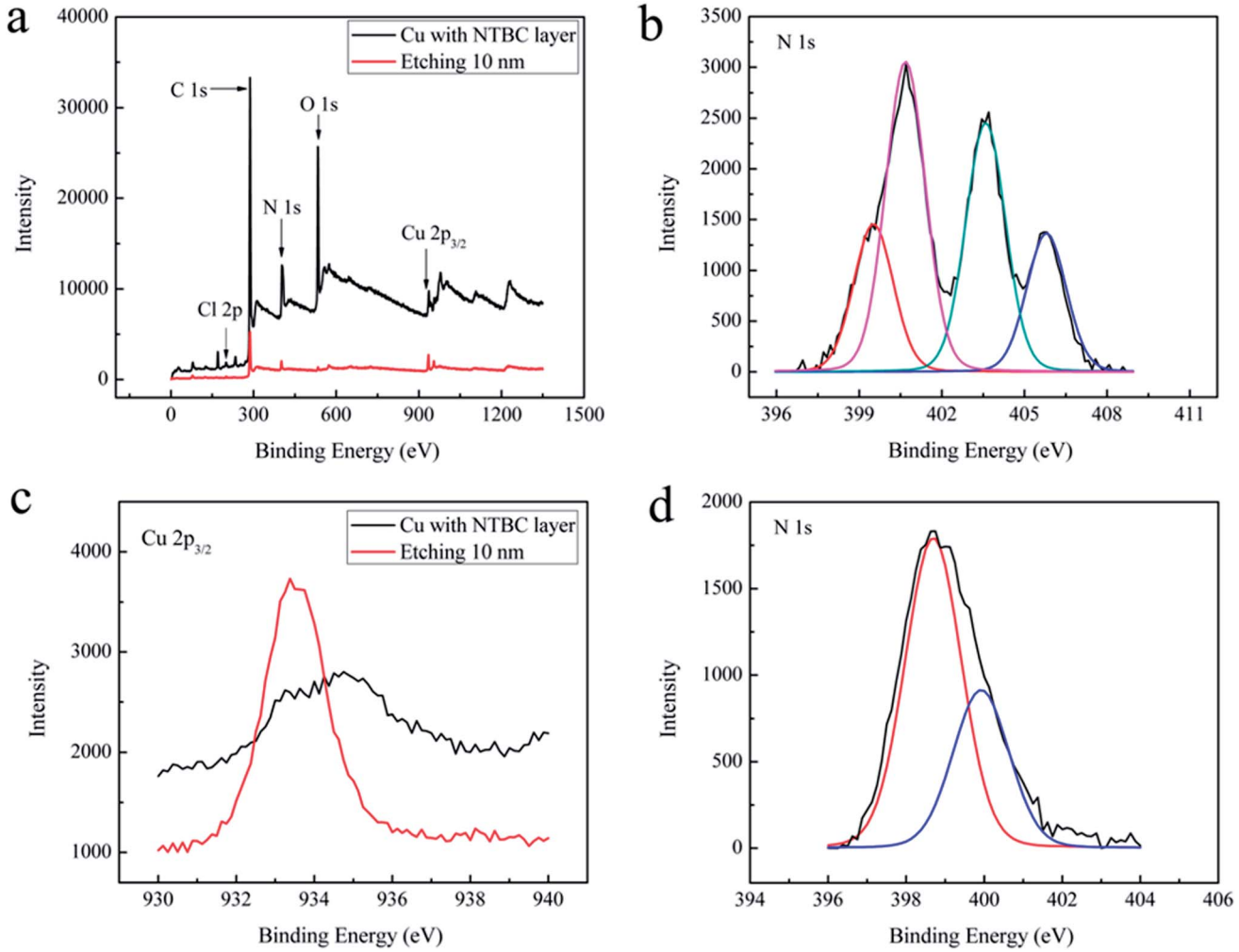


Fig. 2 (a) XPS general spectra of the copper surface after 24 hours of immersion in the 1000 ppm NTBC aqueous solution, (b) high resolution peaks of N1s from the original immersed copper surface, (c) high resolution peaks of Cu2p of the immersed copper surface and a 10.0 nm depth of the copper surface, (d) the detailed XPS peak of N1s after a 10.0 nm etching of the immersed copper surface.

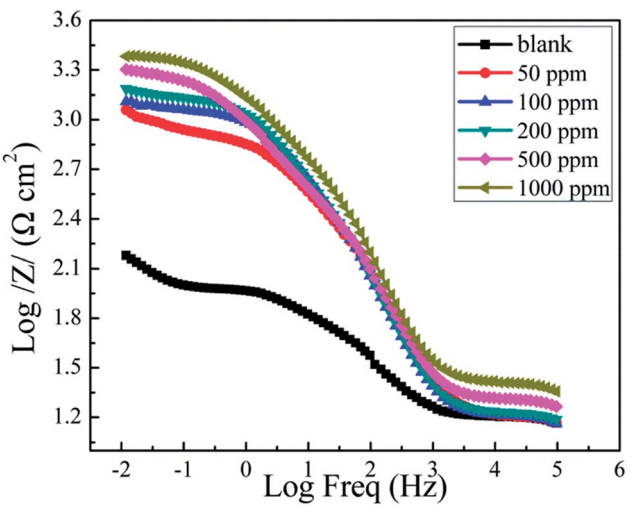


Fig. 3 Bode magnitude plots for copper in 0.1 M $H_2SO_4$ in the absence and presence of different concentrations of NTBC.

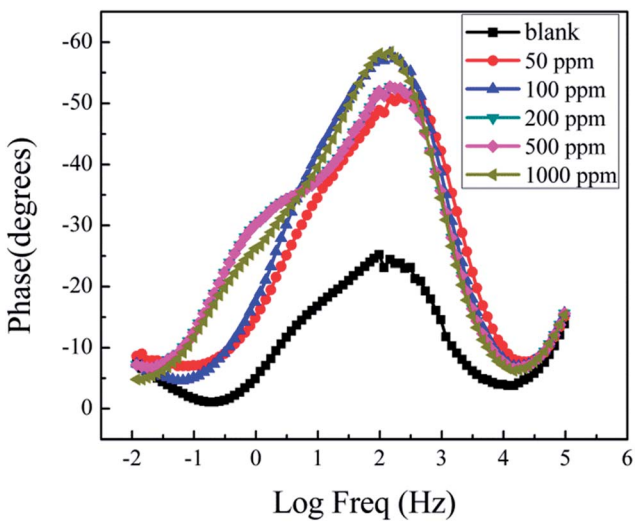


Fig. 4 Bode magnitude plots for copper in 0.1 M $H_2SO_4$ in the absence and presence of different concentrations of NTBC.

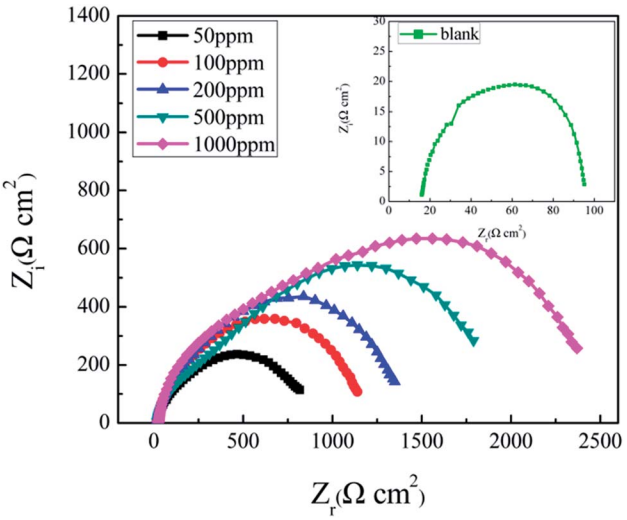


Fig. 5 Nyquist plots for copper in 0.1 M $H_2SO_4$ in the absence and presence of different concentrations of NTBC.

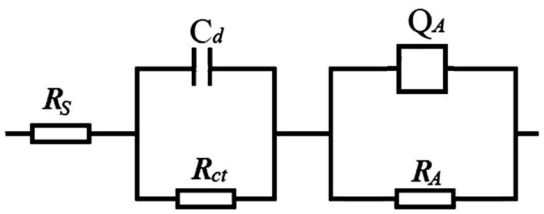


Fig. 6 The electrical equivalent circuit for EIS measurement of copper in 0.1 M $H_2SO_4$ in the absence and presence of different concentrations of NTBC.

NTBC on copper in $H_2SO_4$ medium was enhanced with increasing corrosion inhibitor concentrations.

All the curves displayed in Fig. 5 were approximated by a single capacitive semicircle, suggesting that the corrosion process of copper in $H_2SO_4$ medium was mainly charge-transfer controlled. Overall, the shapes of the curves for all of samples under various concentrations of NTBC were very similar throughout the whole concentration studied in this work. This suggested that almost no change in the corrosion mechanism occurred due to the change of NTBC concentration.

According to the impedance parameters displayed in Table 1, the values of $R_{ct}$ increased from 27.94 Ω $cm^2$ to 286.40 Ω $cm^2$ with the addition of inhibitor, whereas the values of $R_A$ increased from 782.2 Ω $cm^2$ to 2167.0 Ω $cm^2$. Thus, a reduction in corrosion rate and an increase of adsorption quantity occurred with the increase of NTBC concentration. In addition, the inhibition efficiency ($\eta_I$) was enhanced by increasing NTBC concentration, reaching above 70% at a concentration level of 100 ppm. These results all indicate that NTBC has an effective corrosion inhibition for copper in $H_2SO_4$ medium.

### 3.4. Potentiodynamic polarization measurements

Tafel plots generated from potentiodynamic polarization curves for copper in 0.1 M $H_2SO_4$ with various concentrations (from 50 ppm to 1000 ppm) of NTBC as inhibitor at 298 K are shown in Fig. 7. A prominent decrease of the corrosion rate occurred because of the addition of NTBC in $H_2SO_4$ medium.

The corrosion parameters, including corrosion potential ($E_{corr}$), corrosion current density ($i_{corr}$), Tafel slope values ($b_a$ and $b_c$) and inhibition efficiency ($\eta_p$) obtained from the curves in Fig. 7 are summarized in Table 2.

The initial addition of NTBC (50 ppm) causes a sharp reduction of the current density ($i_{corr}$), and $i_{corr}$ decreased further with higher concentrations of the inhibitor. This trend was in accord with the results of EIS, and furthermore confirmed the prediction of the MD stimulation. It was also

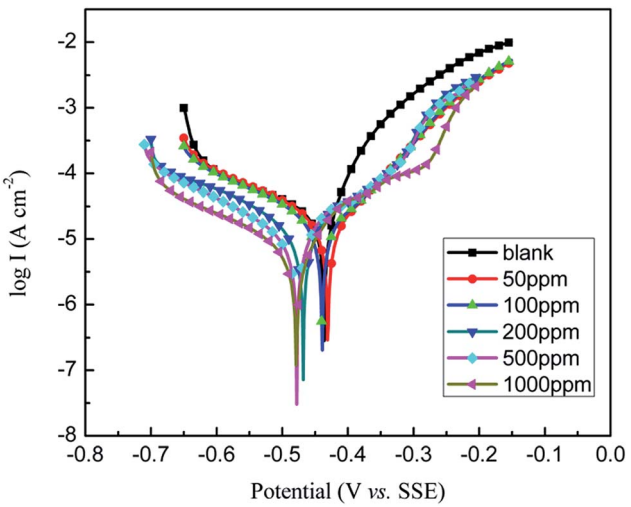


Fig. 7 Tafel plots for copper in 0.1 M $H_2SO_4$ in absence and presence of different concentrations of NTBC.

Table 1 Corrosion inhibition effect of NTBC on copper in $H_2SO_4$ medium with different concentrations of NTBC (EIS studies)

| Concentration of NTBC (ppm) | $R_s$ (Ω $cm^2$) | $C_d$ (F $cm^{-2}$) | $R_{ct}$ (Ω $cm^2$) | $\eta_I$ (%) | $Q_A$ (F $cm^{-2}$) | $R_A$ (Ω $cm^2$) | $n$ |
|---|---|---|---|---|---|---|---|
| 0 | 15.64 | $1.382 \times 10^{-3}$ | 27.94 | — | — | — | 0.7514 |
| 50 | 14.85 | $2.889 \times 10^{-5}$ | 66.12 | 57.74 | $1.405 \times 10^{-4}$ | 782.2 | 0.7062 |
| 100 | 15.30 | $3.903 \times 10^{-5}$ | 93.81 | 70.22 | $1.024 \times 10^{-4}$ | 1064.0 | 0.7661 |
| 200 | 15.92 | $3.635 \times 10^{-5}$ | 91.31 | 69.40 | $1.110 \times 10^{-4}$ | 1297.0 | 0.7533 |
| 500 | 18.83 | $2.565 \times 10^{-5}$ | 137.10 | 79.62 | $2.360 \times 10^{-4}$ | 1856.0 | 0.6634 |
| 1000 | 23.82 | $2.103 \times 10^{-5}$ | 286.40 | 90.24 | $1.674 \times 10^{-4}$ | 2167.0 | 0.6883 |

Table 2 Potentiodynamic polarization curves of copper in $H_2SO_4$ medium with various concentrations of NTBC

| Concentration of NTBC (ppm) | $I_{corr}$ (μA) | $E_{corr}$ (mV) | $b_c$ (mV dec$^{-1}$) | $b_a$ (mV dec$^{-1}$) | $\eta_p$ (%) |
|---|---|---|---|---|---|
| 0 | 33.9188 | −439.728 | −181.4 | 125.1 | — |
| 50 | 18.9489 | −431.264 | −215.6 | 91.4 | 44.13 |
| 100 | 18.4392 | −439.900 | −207.6 | 87.1 | 45.63 |
| 200 | 13.7124 | −469.435 | −254.4 | 83.4 | 59.57 |
| 500 | 11.5332 | −479.329 | −204.8 | 94.3 | 66.00 |
| 1000 | 7.2759 | −479.873 | −218.6 | 209.8 | 78.55 |

observed that the addition of NTBC shifted $E_{corr}$ values in both the anodic and cathodic directions. The analysis of anodic ($b_a$) and cathodic ($b_c$) Tafel slope values indicated that both the anodic and cathodic reactions were suppressed with the addition of NTBC as inhibitor. $i_{corr}$ decreased remarkably, whereas $\eta_p$ increased with increasing NTBC concentration. No definite trend for the shift of $E_{corr}$ under the presence of NTBC can be detected however.

### 3.5. SEM surface morphological examination

The corrosion inhibition effect of NTBC on copper surface was also investigated by corrosion experiments, in which copper with a polished surface was immersed into 0.1 M $H_2SO_4$ containing various concentration of NTBC. Morphologies of these copper substrates after corrosion for 24 hours at 298 K were observed by SEM. The SEM images of polished copper surface before and after corrosion tests are shown in Fig. 8 and 9, respectively.

The original polished copper surface displays a smooth, uniform morphology. After immersion into 0.1 M $H_2SO_4$ for 24 hours at 298 K and in the absence of NTBC, the copper foil was seriously corroded, demonstrating a significantly deteriorated morphology (Fig. 9(a)). However, with the addition of NTBC, the corrosion was obviously inhibited as the roughness of the copper surface reducing sharply according to the images shown in Fig. 9(a)–(f). Moreover, the inhibition effect was enhanced with the increase of NTBC concentration. These results further confirm that NTBC is a very effective inhibitor for the corrosion of copper in $H_2SO_4$ solutions. The similarities of the copper surface morphologies after immersion in $H_2SO_4$ solutions containing 500 ppm and 1000 ppm for 24 hours indicate that 500 ppm is the saturated concentration for NTBC as an inhibitor.

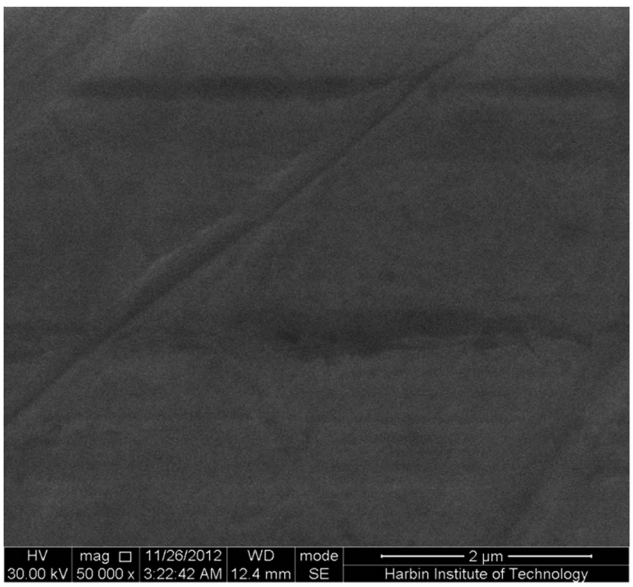


Fig. 8 SEM images of the top view of original polished copper surface before corrosion measurements.

### 3.6. Quantum chemical calculations

According to the results of electrochemical measurements and corrosion experiments, NTBC has been verified as an effective species to inhibit the corrosion of copper in 0.1 M $H_2SO_4$ solutions. Quantum chemical calculations were employed to reveal the relationship between the molecular structures and electronic properties of NTBC, and the corrosion inhibition effects. Localization of the HOMO, the LUMO and the Fukui function distribution were calculated to investigate the electronic properties of NTBC. The optimized structure of NTBC with atom label symbols is shown in Fig. 10.

Based on the frontier molecular orbital theory, the formation of a transition state arises from interactions occurring between the frontier orbitals (HOMO and LUMO) of reacting species.[47] The HOMO and LUMO energies are always closely associated with the electron donating ability and electron accepting ability of the species, respectively. The higher value of $E_{HOMO}$ and the lower value of $E_{LUMO}$ indicate the tendency of the molecule to donate and accept electrons, respectively. The energy gap ($\Delta E$) and the value difference of $E_{HOMO}$ and $E_{LUMO}$ are important parameters to characterize the absorption ability of NTBC on the copper surface.[46,77] The localization of HOMO and LUMO of NTBC are shown in Fig. 11.

The heterocyclic nitrogen (N) of NTBC in Fig. 11(a) displayed a significant contribution to the HOMO. For this reasons the N=N regions and aminoazobenzene region were the main contributors to the HOMO, demonstrating that the preferred active sites for electrophilic attack were located within these regions. The LUMO of NTBC, displayed in Fig. 11(b), was similar to the distribution of HOMO in NTBC. These results suggest that the N=N regions or aminoazobenzene region of NTBC are the probable reactive sites for the adsorption of NTBC on the copper surface.

The nucleophilic/electrophilic sites (susceptible atoms and regions) in the molecular structures of NTBC were localized by the Fukui function. The condensed Fukui functions were found by taking the finite difference approximations from the population analysis of atoms in molecules, depending on the direction of the electron transfer. The equations used for electrophilic attack, nucleophilic attack, and radical attack were eqn (4), (5), and (6), respectively.[28,47,77,78]

 

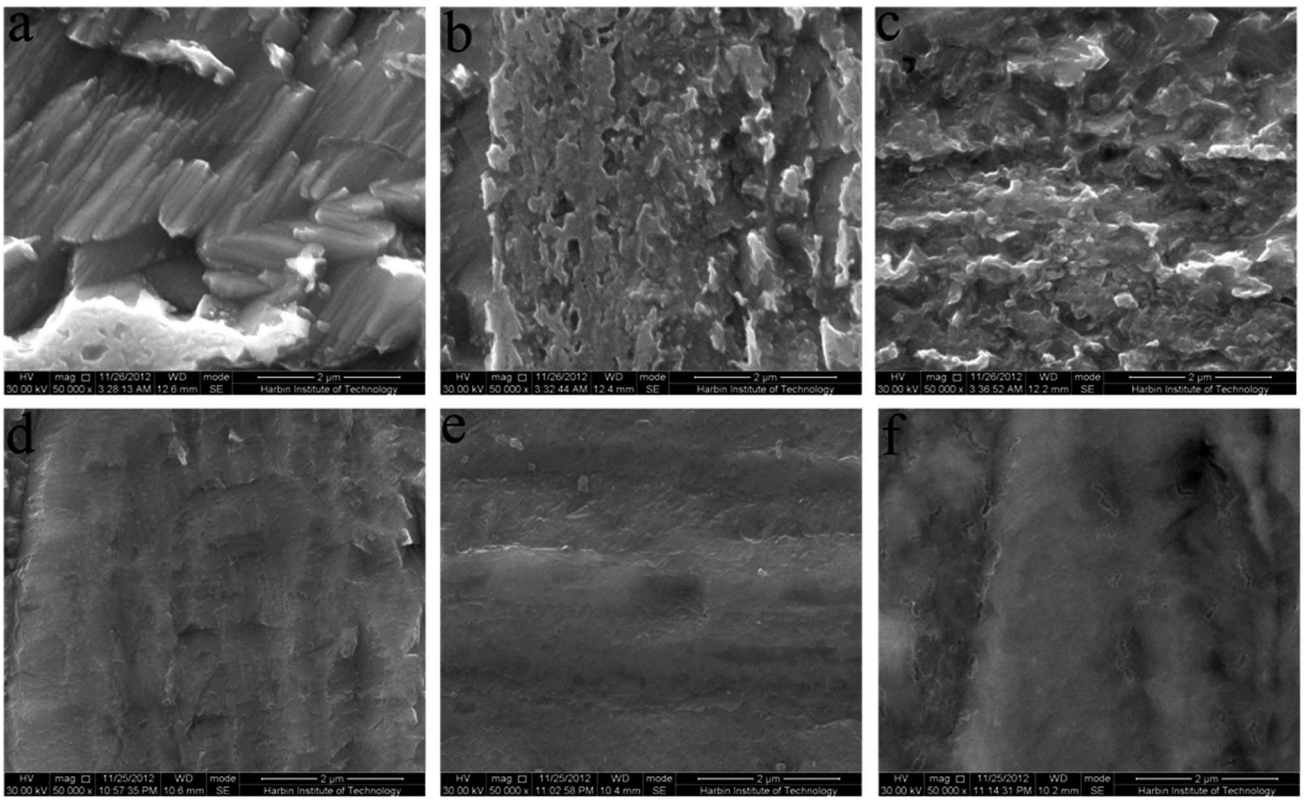


Fig. 9 SEM images of the top view of polished copper foils immersed into 0.1 M $H_2SO_4$ containing various concentrations of NTBC for 24 hours at 298 K. (a) 0 ppm, (b) 50 ppm, (c) 100 ppm, (d) 200 ppm, (e) 500 ppm, and (f) 1000 ppm.

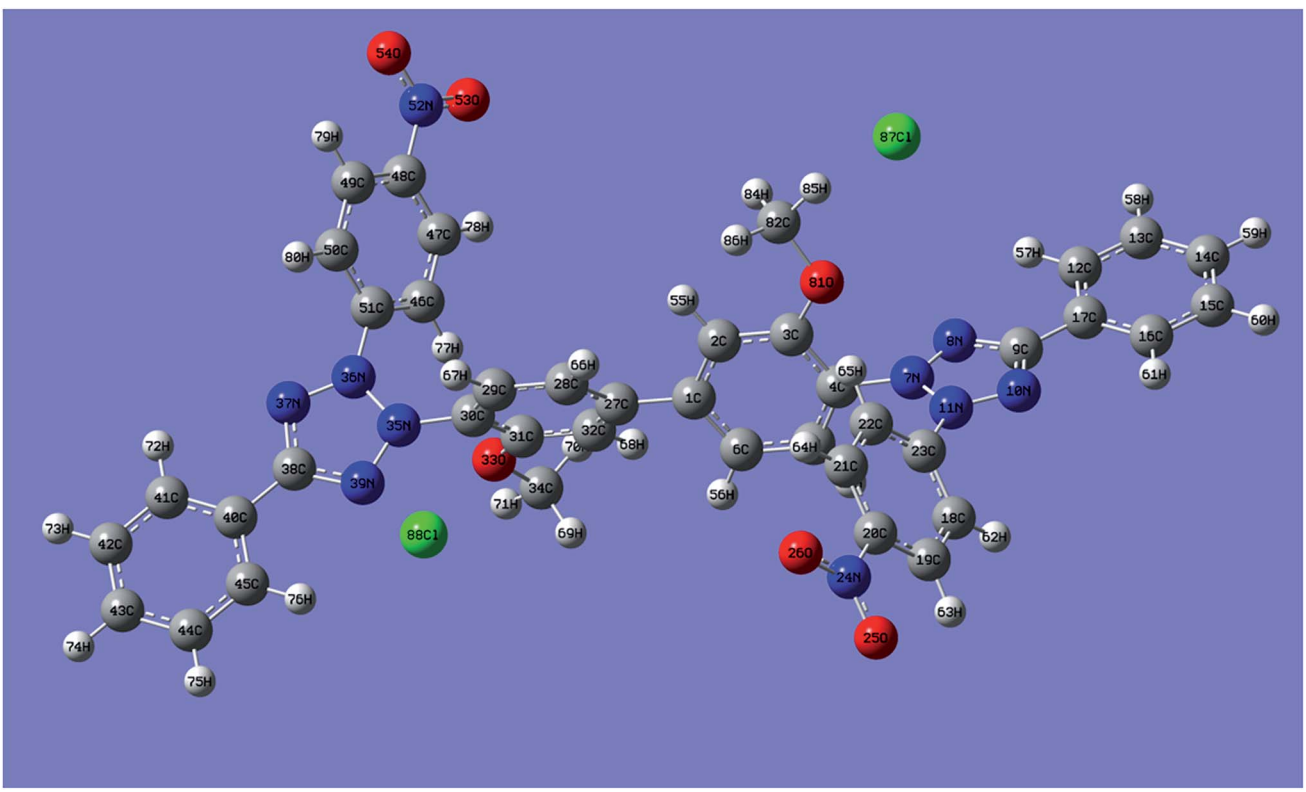


Fig. 10 Optimized structure of NTBC with atom label symbols.

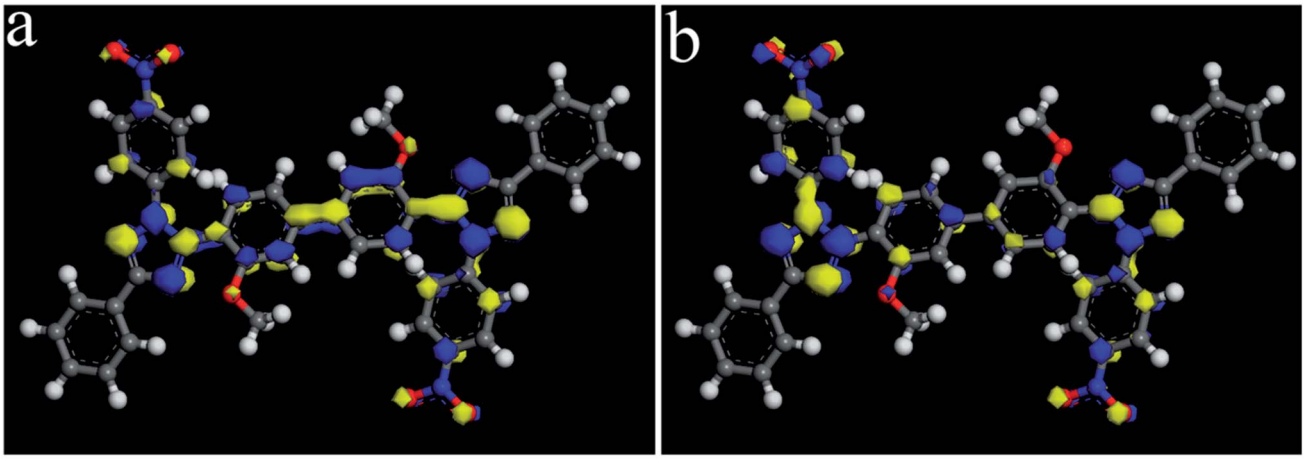


Fig. 11 Localization of HOMO and LUMO of $NTB^{2+}$ calculated by DFTB+, (a) HOMO, (b) LUMO.

$$f_i^- = q_i(N) - q_i(N-1) \quad (4)$$

$$f_i^+ = q_i(N+1) - q_i(N) \quad (5)$$

$$f_i^0 = \frac{q_i(N+1) + q_i(N-1)}{2} \quad (6)$$

where $q_i$ is the gross charge of atom 'i' in the NTBC molecules. It has been found that the sites with the highest values of $f^+$, $f^-$, and $f^0$ in molecular structure were the most susceptible sites for the nucleophilic, electrophilic attacks, and radical attack, severally. These Fukui functions determined the direction of the electron transfer in the interactions between the adsorbed NTBC molecules and copper surfaces. The Fukui function distributions in NTBC were shown in Fig. 12 and Fukui functions of nitrogen and oxygen atoms in NTBC were listed in Table 3.

The Fukui functions in Fig. 12 and Table 3 further show that the N atoms in the imidazole ring are the most susceptible sites for the electrophilic attacks, as they present the highest values of $f^-$. On the other hand, the N atoms in the imidazole ring are also the most susceptible sites for the nucleophilic attacks based on their highest values of $f^+$. The electrophilic attack plays a leading role in the adsorption of organic molecules on metal surfaces. Therefore, the N=C–N and N=N regions in the imidazole ring were the most active reaction sites, and the NTBC molecule could adsorb directly on the copper surface through the sharing of electrons between the nitrogen atoms and copper atoms.

According to the quantum chemical calculations and molecular dynamic simulations, the inhibition effect of NTBC on copper corrosion derives from the strong adsorption of NTBC on the copper surface. The inhibition efficiency increases with increasing electron-donating ability at the copper surface. On the basis of these calculations, it is expected that NTBC serves as a donor of electrons, and the copper surface the acceptor. In these experiments, NTBC thereby acts as an effective inhibitor by binding to the copper surface, forming strong N–Cu chemical bonds in deprotonated form, and then forming an adsorption layer on the copper surface. The results of quantum chemical calculations further confirmed that there is more than one bond to the copper surface per NTBC molecule, as there are multiple groups with nitrogen to form strong N–Cu chemical bonds.

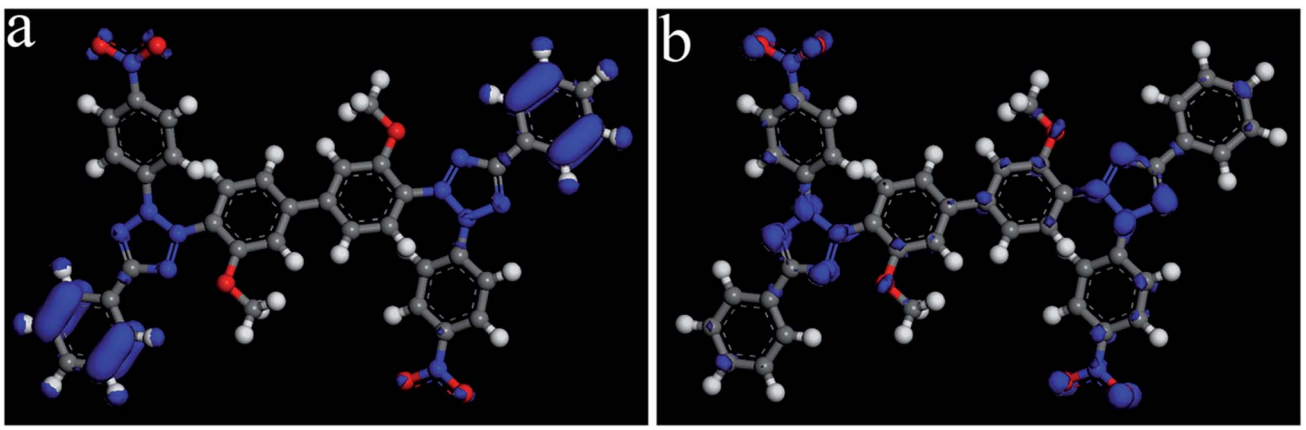


Fig. 12 The Fukui function distributions in $NTB^{2+}$. (a) Fukui function for electrophilic attack ($f^-$), (b) Fukui functions for nucleophilic attack ($f^+$).

 

Table 3 Mulliken Fukui functions calculated for the nitrogen and oxygen atoms of NTBC (numbers of atoms were shown in Fig. 10)

| Atoms | $f^+$ | $f^0$ | $f^-$ |
|---|---|---|---|
| 7 N | 0.011 | 0.008 | 0.005 |
| 8 N | 0.027 | 0.015 | 0.004 |
| 10 N | 0.035 | 0.021 | 0.008 |
| 11 N | 0.015 | 0.010 | 0.006 |
| 24 N | 0.005 | 0.005 | 0.005 |
| 25 O | 0.038 | 0.031 | 0.023 |
| 26 O | 0.032 | 0.027 | 0.022 |
| 33 O | 0.011 | 0.005 | 0.000 |
| 35 N | 0.015 | 0.010 | 0.005 |
| 36 N | 0.015 | 0.011 | 0.007 |
| 37 N | 0.037 | 0.023 | 0.008 |
| 39 N | 0.034 | 0.018 | 0.003 |
| 52 N | 0.007 | 0.004 | 0.001 |
| 53 O | 0.035 | 0.025 | 0.015 |
| 54 O | 0.044 | 0.032 | 0.019 |
| 81 O | 0.010 | 0.006 | 0.001 |

## 4. Conclusion

NTBC was predicted to be an effective inhibitor for copper corrosion in $H_2SO_4$ solution through a theoretical study *via* MD simulation. XPS spectra further verified an effective adsorption of NTBC on the copper surface. Based on the EIS results, the NTBC increased the whole resistance of copper corrosion process by forming an absorption layer on copper surface. Potentiodynamic polarization curves confirmed that the corrosion rate decreased prominently with the addition of NTBC in $H_2SO_4$ solution, as the increasing concentration of NTBC caused a decreasing current density ($i_{corr}$). Morphology observation directly support that the corrosion of copper was inhibited due to the addition of NTBC surface. The optimal concentration of NTBC as an inhibitor for the corrosion of copper in 0.1 M $H_2SO_4$ solutions was 500 ppm. According to the quantum chemical calculations, the N atoms in the imidazole ring and the O atoms in the branched chain were found the most active adsorption sites binding to the copper surface.

## Acknowledgements

The authors are grateful for financial support from the State Key Laboratory of Urban Water Resource and Environment (Harbin Institute of Technology) (2012DX03).

## Notes and references

1 D. T. Read, Y. W. Cheng and R. Geiss, *Microelectron. Eng.*, 2004, **75**, 63–70.
2 S. Miura and H. Honma, *Surf. Coat. Technol.*, 2003, **169–170**, 91–95.
3 S. John, J. Joy, M. Prajila and A. Joseph, *Mater. Corros.*, 2011, **62**, 1031–1041.
4 M. Finšgar and I. Milošev, *Corros. Sci.*, 2010, **52**, 2737–2749.
5 E. M. Sherif and S.-M. Park, *Electrochim. Acta*, 2006, **51**, 4665–4673.
6 A. Döner, A. O. Yüce and G. Kardaş, *Ind. Eng. Chem. Res.*, 1998, **52**, 9709–9718.
7 A. Kokalj, S. Peljhan, M. Finšgar and I. Milošev, *J. Am. Chem. Soc.*, 2010, **132**, 16657–16668.
8 S. Deng, X. Li and H. Fu, *Corros. Sci.*, 2010, **52**, 3840–3846.
9 C. M. Murira, C. Punckt, H. C. Schniepp, B. Khusid and I. A. Aksay, *Langmuir*, 2008, **24**, 14269–14275.
10 Y.-C. Pan, Y. Wen, L.-Y. Xue, X.-Y. Guo and H.-F. Yang, *J. Phys. Chem. C*, 2012, **116**, 3532–3538.
11 E.-S. M. Sherif, R. M. Erasmus and J. D. Comins, *J. Colloid Interface Sci.*, 2007, **306**, 96–104.
12 Y. Tang, X. Yang, W. Yang, Y. Chen and R. Wan, *Corros. Sci.*, 2010, **52**, 242–249.
13 G. Gece, *Corros. Sci.*, 2008, **50**, 2981–2992.
14 Z. Chen, L. Huang, G. Zhang, Y. Qiu and X. Guo, *Corros. Sci.*, 2012, **65**, 214–222.
15 A. Döner, A. O. Yüce and G. Kardaş, *Ind. Eng. Chem. Res.*, 2013, **52**, 9709–9718.
16 S. Shen, C.-d. Zhu, X.-y. Guo, C.-c. Li, Y. Wen and H.-F. Yang, *RSC Adv.*, 2014, **4**, 10597–10606.
17 K. F. Khaled, *Mater. Chem. Phys.*, 2008, **112**, 104–111.
18 R. A. Friesner, *Proc. Natl. Acad. Sci. U. S. A.*, 2005, **102**, 6648–6653.
19 H. Li, Y. Li and M. Chen, *RSC Adv.*, 2013, **3**, 12133–12139.
20 H. J. Kulik, N. Luehr, I. S. Ufimtsev and T. J. Martinez, *J. Phys. Chem. B*, 2012, **116**, 12501–12509.
21 P. Söderhjelm, F. Aquilante and U. Ryde, *J. Phys. Chem. B*, 2009, **113**, 11085–11094.
22 M. Remko, R. Broer and A. Remkova, *RSC Adv.*, 2014, **4**, 8072–8084.
23 S. Bhattacharyya and K. Hatua, *RSC Adv.*, 2014, **4**, 18702–18709.
24 V. Van Speybroeck and R. J. Meier, *Chem. Soc. Rev.*, 2003, **32**, 151–157.
25 Z. Zhang, K. Yan and J. Zhang, *RSC Adv.*, 2013, **3**, 6401–6407.
26 G. Meleshko, J. Kulhavy, A. Paul, D. J. Willock and J. A. Platts, *RSC Adv.*, 2014, **4**, 7003–7012.
27 V. Tsui and D. A. Case, *J. Am. Chem. Soc.*, 2000, **122**, 2489–2498.
28 H. Shokry, *J. Mol. Struct.*, 2014, **1060**, 80–87.
29 C. Chen, W. Lei, M. Xia, F. Wang and X. Gong, *Desalination*, 2013, **309**, 208–212.
30 B. C. Stephenson, A. Goldsipe and D. Blankschtein, *J. Phys. Chem. B*, 2008, **112**, 2357–2371.
31 S. C. Ammal and A. Heyden, *J. Phys. Chem. Lett.*, 2012, **3**, 2767–2772.
32 K. Furse and S. Corcelli, *J. Phys. Chem. Lett.*, 2010, **1**, 1813–1820.
33 G. Gece and S. Bilgiç, *Corros. Sci.*, 2009, **51**, 1876–1878.
34 M. G. V. Satyanarayana, V. Himabindu, Y. Kalpana, M. Ravi Kumar and K. Kumar, *J. Mol. Struct.*, 2009, **912**, 113–118.
35 J. Zhang, G. Qiao, S. Hu, Y. Yan, Z. Ren and L. Yu, *Corros. Sci.*, 2011, **53**, 147–152.
36 T. H. Muster, A. E. Hughes, S. A. Furman, T. Harvey, N. Sherman, S. Hardin, P. Corrigan, D. Lau, F. H. Scholes,

P. A. White, M. Glenn, J. Mardel, S. J. Garcia and J. M. C. Mol, *Electrochim. Acta*, 2009, **54**, 3402–3411.
37 M. Lebrini, M. Traisnel, M. Lagrenée, B. Mernari and F. Bentiss, *Corros. Sci.*, 2008, **50**, 473–479.
38 T. Arslan, F. Kandemirli, E. E. Ebenso, I. Love and H. Alemu, *Corros. Sci.*, 2009, **51**, 35–47.
39 P. Zhao, Q. Liang and Y. Li, *Appl. Surf. Sci.*, 2005, **252**, 1596–1607.
40 G. Gece and S. Bilgiç, *Corros. Sci.*, 2010, **52**, 3435–3443.
41 A. Y. Musa, R. T. T. Jalgham and A. B. Mohamad, *Corros. Sci.*, 2012, **56**, 176–183.
42 A. Y. Musa, A. A. H. Kadhum, A. B. Mohamad and M. S. Takriff, *Mater. Chem. Phys.*, 2011, **129**, 660–665.
43 B. Xu, W. Yang, Y. Liu, X. Yin, W. Gong and Y. Chen, *Corros. Sci.*, 2014, **78**, 260–268.
44 D. Turcio-Ortega, T. Pandiyan, J. Cruz and E. Garcia-Ochoa, *J. Phys. Chem. C*, 2007, **111**, 9853–9866.
45 W. Wang, Z. Li, Q. Sun, A. Du, Y. Li, J. Wang, S. Bi and P. Li, *Corros. Sci.*, 2012, **61**, 101–110.
46 S. Xia, M. Qiu, L. Yu, F. Liu and H. Zhao, *Corros. Sci.*, 2008, **50**, 2021–2029.
47 L. Feng, H. Yang and F. Wang, *Electrochim. Acta*, 2011, **58**, 427–436.
48 L. M. Rodríguez-Valdez, A. Martínez-Villafañe and D. Glossman-Mitnik, *J. Mol. Struct.*, 2005, **713**, 65–70.
49 Y. Yan, X. Wang, Y. Zhang, P. Wang, X. Cao and J. Zhang, *Corros. Sci.*, 2013, **73**, 123–129.
50 J. Zhang, W. Yu, L. Yu, Y. Yan, G. Qiao, S. Hu and Y. Ti, *Corros. Sci.*, 2011, **53**, 1331–1336.
51 Y. Tang, X. Yang, W. Yang, R. Wan, Y. Chen and X. Yin, *Corros. Sci.*, 2010, **52**, 1801–1808.
52 K. F. Khaled, M. H. Hamed, K. M. Abdel-Azim and N. S. Abdelshafi, *J. Solid State Chem.*, 2011, **15**, 663–673.
53 K. F. Khaled, *Electrochim. Acta*, 2008, **53**, 3484–3492.
54 K. F. Khaled and M. A. Amin, *Corros. Sci.*, 2009, **51**, 1964–1975.
55 H. Sun, *J. Phys. Chem. B*, 1998, **102**, 7338–7364.
56 J. Pozuelo, E. Riande, E. Saiz and V. Compañ, *Macromolecules*, 2006, **39**, 8862–8866.
57 K. Mazeau and L. Heux, *J. Phys. Chem. B*, 2003, **107**, 2394–2403.
58 H. Heinz, B. L. Farmer, R. B. Pandey, J. M. Slocik, S. S. Patnaik, R. Pachter and R. R. Naik, *J. Am. Chem. Soc.*, 2009, **131**, 9704–9714.
59 T. Frauenheim, G. Seifert, M. Elstner, T. Niehaus, C. Köhler, M. Amkreutz, M. Sternberg, Z. Hajnal, A. Di Carlo and S. Suhai, *J. Phys.: Condens. Matter*, 2002, **14**, 3015–3047.
60 M. Elstner, D. Porezag, G. Jungnickel, J. Elsner, M. Haugk, T. Frauenheim, S. Suhai and G. Seifert, *Phys. Rev. B: Condens. Matter Mater. Phys.*, 1998, **58**, 7260–7268.
61 A. Di Carlo, M. Gheorghe, P. Lugli, M. Sternberg, G. Seifert and T. Frauenheim, *Phys. B*, 2002, **314**, 86–90.
62 M. Elstner, P. Hobza, T. Frauenheim, S. Suhai and E. Kaxiras, *J. Chem. Phys.*, 2001, **114**, 5149–5155.
63 M. Elstner, T. Frauenheim, E. Kaxiras, G. Seifert and S. Suhai, *Phys. Status Solidi B*, 2000, **217**, 357–376.
64 S. Goedecker and C. J. Umrigar, *Phys. Rev. A: At., Mol., Opt. Phys.*, 1997, **55**, 1765–1771.
65 I. C. Lin, A. P. Seitsonen, I. Tavernelli and U. Rothlisberger, *J. Chem. Theory Comput.*, 2012, **8**, 3902–3910.
66 S. Kozuch, D. Gruzman and J. M. L. Martin, *J. Phys. Chem. C*, 2010, **114**, 20801–20808.
67 A. Kokalj, *Corros. Sci.*, 2013, **70**, 294–297.
68 C. D. Batich and D. S. Donald, *J. Am. Chem. Soc.*, 1984, **106**, 2758–2761.
69 Y. Yamamoto and H. Konno, *Bull. Chem. Soc. Jpn.*, 1987, **60**, 1299–1302.
70 M. Seno, S. Tsuchiya and S. Ogawa, *J. Am. Chem. Soc.*, 1977, **99**, 3014–3018.
71 M. Ahmed, J. A. Byrne and J. A. D. McLaughlin, *e-J. Surf. Sci. Nanotechnol.*, 2009, **7**, 217–224.
72 M. Camalli, F. Caruso, G. Mattogno and E. Rivarola, *Inorg. Chim. Acta*, 1990, **170**, 225–231.
73 M. Döring, M. Rudolph, E. Uhlig, V. I. Nefedov and I. V. Salyn, *Z. Anorg. Allg. Chem.*, 1986, **532**, 65–72.
74 S. J. Yuan, S. O. Pehkonen, Y. P. Ting, E. T. Kang and K. G. Neoh, *Ind. Eng. Chem. Res.*, 2008, **47**, 3008–3020.
75 D. A. López, S. N. Simison and S. R. de Sánchez, *Corros. Sci.*, 2005, **47**, 735–755.
76 B. V. Appa Rao and K. Chaitanya Kumar, *J. Mater. Sci. Technol.*, 2014, **30**, 65–76.
77 C. Wang, J. Zhang, P. Yang and M. An, *Electrochim. Acta*, 2013, **92**, 356–364.
78 N. O. Eddy, *J. Adv. Res.*, 2011, **2**, 35–47.

 